Regional Remote Sensing Analysis of Fault Tectonics in the Northwestern Part of the Verkhoyan-Kolyma Orogenic Region and Assessment of Its Role in Ore Formation

V. A. Minaev[1]*, S. A. Ustinov[1], V. A. Petrov[1], A. D. Svecherevsky[1], I. O. Nafigin[1], A. I. Manevich[2], and D. Zh. Akmatov[2]

[1]Institute of Geology of Ore Deposits, Petrography, Mineralogy and Geochemistry (IGEM) RAS, Moscow, Russia
[2]The Geophysical Center of the Russian Academy of Sciences (GC) RAS, Moscow, Russia
* **Correspondence to:** Vasilii Minaev, minaev2403@mail.ru

Abstract: The article presents the results of a comprehensive analysis of fault tectonics in the northwestern part of the Verkhoyan-Kolyma orogenic region. The studies were performed on a regional scale. Based on a digital relief model, lineaments were identified manually and automatically. The results obtained in combination with literature data allowed us to perform tectonophysical reconstructions using the model of P. L. Hancock (1985). Based on the reconstructions, we determined the expected areas of tectonic structures that had the highest hydraulic activity during collision processes, which are presumably associated with gold deposits and ore occurrences in Eastern Yakutia. Areas promising for the discovery of new ore objects were identified.

Citation: Minaev V. A., Ustinov S. A., Petrov V. A., Svecherevsky A. D., Nafigin I. O., Manevich A. I., and Akmatov D. Zh. (2025), Regional Remote Sensing Analysis of Fault Tectonics in the Northwestern Part of the Verkhoyan-Kolyma Orogenic Region and Assessment of Its Role in Ore Formation , *Russian Journal of Earth Sciences*, 25, ES4010, EDN: HHENIS, https://doi.org/10.2205/2025es001039

Introduction

The territory of Eastern Yakutia is currently considered one of the most promising in terms of discovering new gold ore objects, including large and super-large deposits [*Antonov and Gamyanin*, 2021; *Volkov*, 2016]. At the same time, a significant part of the known large objects were identified in the southeastern part of the Verkhoyan-Chersky orogenic belt (Dora-Pil, Tallalakh, Malotarynskoye deposits) and the South Verkhoyansk orogenic belt (Nezhdaninsky ore region, Dybinsky ore cluster, Zaderzhninskoye deposit). The situation is different on the northern continuation of the same metallogenic zones of the Yana-Kolyma orogenic region (Figure 1). In the northern segment of the Verkhoyan-Chersky orogenic belt, the only large deposit Kyuchus, has been discovered, and in the northwest of the Verkhoyan orogenic belt, only a few ore occurrences have been discovered, the most promising of which is Dyandi. This situation is also due to the inaccessibility of these territories for field research.

The main part of gold ore objects of various ranks in the northwestern part of the Verkhoyansk-Kolyma orogenic region are of hydrothermal type. It is known that hydrothermal processes are controlled by fault tectonics [*Cherezov et al.*, 1992]. Thus, we can talk about fault tectonics as one of the most important ore-controlling factors in relation to the studied territory.

There are very few works devoted to the study of the framework of faults for the Verkhoyan-Kolyma orogenic region. A detailed study of fault tectonics and folded structures of the Mesozoic Verkhoyan-Kolyma system is devoted to the work of *Gusev* [1979], from which it follows that the main part of the mapped faults acquired their appearance in the late Mesozoic.
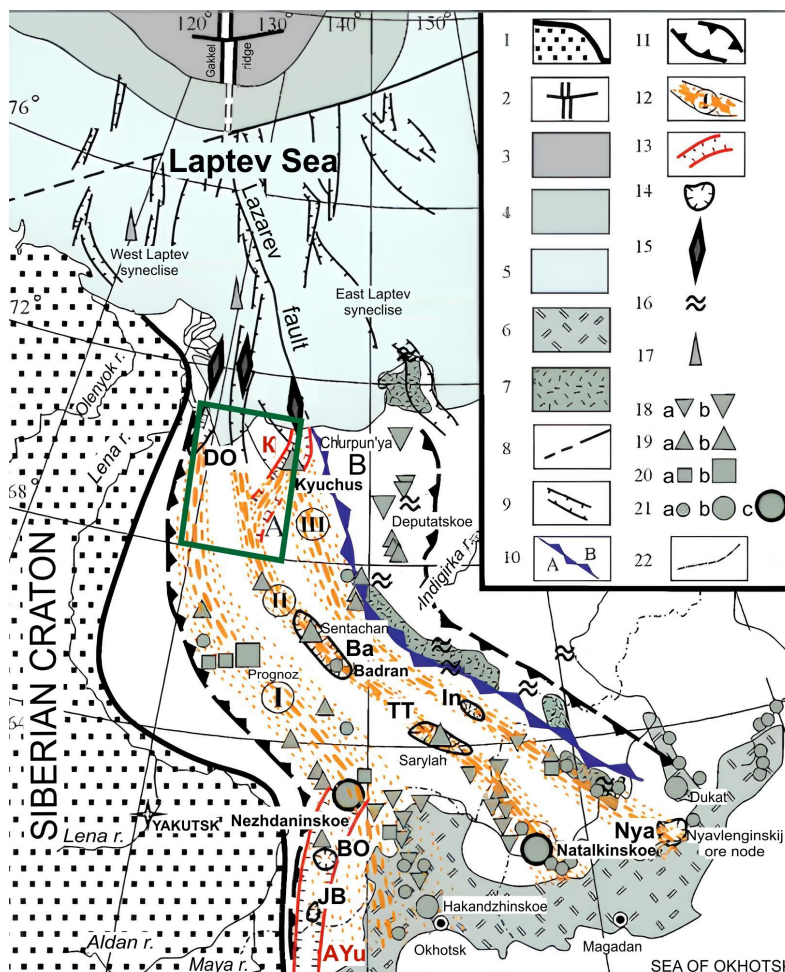
Figure 1. Schematic diagram of metallogenic zones of Eastern Yakutia [after *Antonov and Gamyanin*, 2021] 1 – Siberian craton; 2 – Gakkel Ridge; 3 – Eurasian oceanic basin; 4 – continental slope; 5 – shelf; 6 – Okhotsk-Chukotka marginal-continental Late Cretaceous volcanic belt; 7 – Jurassic volcanic belts; 8 – transform fault; 9 – rift basins. Boundaries: 10 – southwestern (A) and northeastern (B) sectors; 11 – East Yakut metallogenic belt; 12 – metallogenic zones (I – Verkhoyansk, II – Tarynsk, III – Nizhneyansko-Selyannyakhskaya); 13 – metallogenic subzones (K – Kularskaya, AYu – Allah-Yunskaya). 14 – promising ore districts: DO – Dyandinsko-Okhonsoysky; Ba – Badransky; TT – Tuora-Tassky; In – Intakhsky; BO – Bular-Onocholokhsky; JB – Jurassic-Brindakitsky; Nya – Nyavlenginsky. 15 – rifts; 16 – ophiolite massifs; 17 – promising oil and gas bearing areas. Deposits: 18 – Sn, W, Mo (a – small and medium; b – large); 19 – Au, Sb, Hg (a – small and medium; b – large); 20 – Ag, Pb, Zn (a – small and medium; b – large); 21 – Au, Ag (a – small; b – medium; c – large); 22 – administrative boundaries. Green outline – boundaries of the study area.

The above circumstances prompted the authors of this article to analyze the framework of faults in the northwestern part of the Verkhoyan-Kolyma orogenic region using a set of modern methods for processing Earth remote sensing data and tectonophysical reconstructions. The results obtained allowed us to draw up a scheme of potentially promising areas for the discovery of gold ore objects.

Research Region

The Verkhoyansk fold-and-thrust belt formed in the late Paleozoic-Mesozoic on the subsided margin of the Siberian paleocontinent. It is composed of thick terrigenous-sedimentary strata that formed on the shelf, continental slope and foot of the passive margin of the Siberian paleocontinent on the margins of the Okhotsk terrane and the Kolyma-Omolon superterrane (Figure 2).
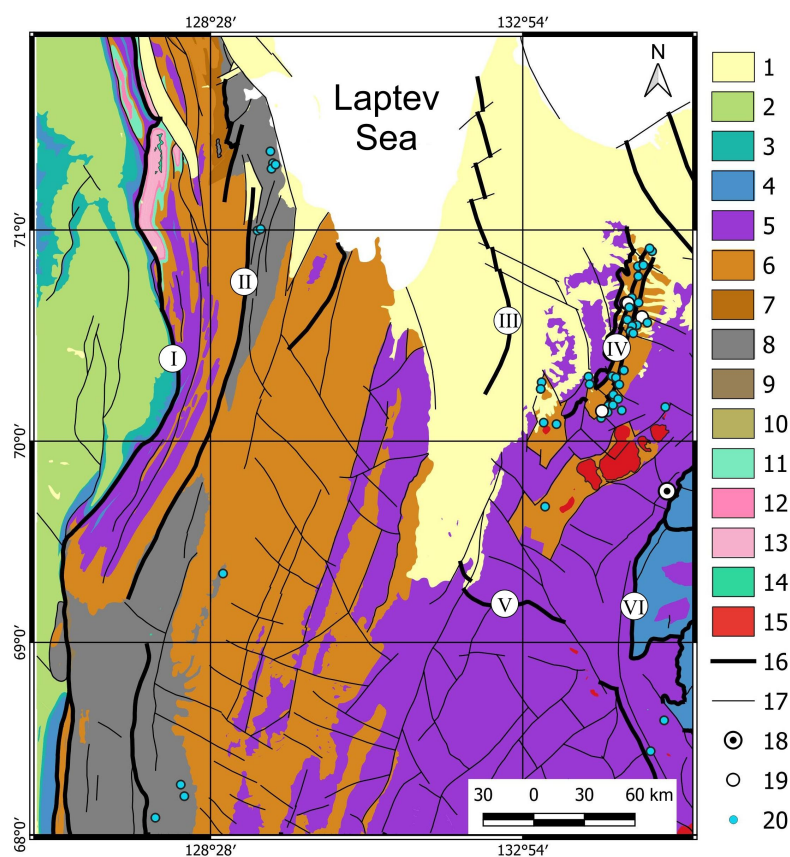
Figure 2. Schematic geological map of the northwestern part of the Verkhoyansk-Kolyma orogenic region (compiled based on the materials of [*Borisova et al.*, 2016, 2020]). 1 – Paleogene-Neogene sediments; 2 – Cretaceous sediments (sands, sandstones, siltstones, mudstones, interlayers and lenses of coal, conglomerates); 3 – Jurassic-Cretaceous sediments (sandstones, siltstones, mudstones, interlayers and lenses of coal); 4 – Jurassic sediments (sandstones, conglomerates, siltstones, mudstones, interlayers and lenses of coal); 5 – Triassic formations (sandstones, limestones, siltstones, mudstones, interlayers of tuffs, gravelites); 6 – Permian sediments (sandstones, siltstones, mudstones, interlayers and lenses of conglomerates); 7 – Carboniferous-Permian sediments (sandstones, siltstones, mudstones); 8 – Carboniferous sediments (sandstones, siltstones, mudstones, conglomerates, dolomites, limestones); 9 – Devonian sediments (sandstones, siltstones, anhydrites, gypsums, limestones, calcareous shales and sandstones, conglomerate lenses); 10 – Silurian-Devonian sediments (limestones and dolomites); 11 – Cambrian sediments (dolomite, conglomerate, sandstone, siltstone, limestone, shales, argillite, trachybasalt covers); 12 – Vendian sediments (dolomite, limestone, sandstone); 13 – Riphean sediments (limestone, dolomites, marl, sandstone, shales, conglomerate lenses); 14 – dikes of basic rocks; 15 – granites, granodiorites, monzogranites; 16 – major faults (I – Priverkhoyansky marginal suture; II – Central Verkhoyansky; III – East Omoloysky; IV – Emiss fault system; V – Adycha-Tarynsky; VI – Yansky); 17 – minor faults; 18 – large gold ore deposit Kyuchus; 19 – small gold ore deposits; 20 – gold occurrences.

To date, there is no generally accepted complete history of the region's development. We will briefly outline its main established stages.

In the Middle – Late Devonian and Early Carboniferous, several rifts formed within the eastern margin of the paleocontinent, leading to the separation of large continental blocks from it, including the Okhotsk and Omolon cratonic terranes, the Prikolymsky and Omulevsky terranes. As a result of rifting, the Oymyakon small ocean basin was formed. After the rifting stage, the east of the Siberian paleocontinent developed in a passive margin regime.

At the very end of the Late Jurassic, the Kolyma-Omolon superterrane collided with the Verkhoyansk passive margin of the Siberian paleocontinent, as a result of which in the Cretaceous the Verkhoyansk terrigenous complex formed a fold-and-thrust orogen containing belts of collisional granitoids [*Kungurtsev and Goshko*, 2023]. At this time, regional shifts were laid with the formation of a fold-and-thrust structure [*Konstantinovsky*, 2007]. It is assumed that noble metal mineralization in the study area is associated with the influence of accretion-collisional processes of the formation of the South Anyui suture and the Novosibirsk-Chukotka orogenic belt (Aptian-Albian time) [*Prokopiev et al.*, 2018]. Considering that mineralization is controlled by fault structures, it can be concluded that the faults acquired their final morphological appearance at the end of the Early Cretaceous (125–105 Ma). It is important that, unlike the North-Eastern sector (see Figure 1), the study region is characterized by metallogenic specialization mainly in Au and less in Sb, Hg, Ag, Pb, Zn [*Antonov and Gamyanin*, 2021]. The Kyuchus Au-Sb-Hg deposit is located in the eastern part of the study area. It is localized in the northwest of the Kular-Nera shale belt (terrane) in the hinterland of the Verkhoyansk fold-and-thrust belt in the zone of influence of the regional Yana fault. To the north are localized small deposits – Mastakh, Kyllakh, Yemelyanovskoye and Emys.

In the western part, the Dyandinsko-Okhonosoi gold ore region deserves special attention, located in the extreme north of the Verkhoyansk metallogenic zone near the Laptev Sea coast among the shales of the Upper Carboniferous – Lower Permian (see Figure 1). The ore region extends in a submeridional direction for a distance of about 90 km with a width of 10–15 km. Ore bodies are represented by veins, as well as stockworks in sandstone layers. The large Dyandi ore occurrence and a significant number of insufficiently studied gold ore occurrences (Nikolaevskoye, Nochka, Otkrytoye, Yasnoye, Shkolnoye, Okhonosoy, etc.) are known here. The strike of the ore-controlling faults is submeridional, conformal to the strike of the metallogenic zone [*Antonov and Gamyanin*, 2021].

Research Methods

The research methodology is described in detail in the works [*Minaev et al.*, 2024; *Ustinov et al.*, 2024], therefore, below we will note only the main most important stages. Lineament analysis of the territory was carried out using a special technique based on the construction and processing of a digital elevation model (DEM), proposed and verified on real geological objects by the employees of the laboratory of Geoinformatics of IGEM RAS [*Ustinov and Petrov*, 2016]. The technique is effective even in areas with weakly dissected relief. The DEM of the territory was created using open data from the radar interferometric survey of the globe's surface ASTER GDEM (Global Digital Elevation Model) of the third version. The work used a model with a generalization level of 1 km/pixel. The choice of the DEM generalization level is determined by the aim of the work and, in accordance with it, the scale level of the available geological materials

The survey results are raster images with the values of the relief elevation marks for each pixel in GeoTIFF format, containing metadata on the georeferencing. The lineaments on the DEM were identified using software based on neural network technologies developed with the participation of individual authors of this article [*Grishkov et al.*, 2023].

The general principles of operation of this software are based on the fundamental concepts of the functioning of neural networks and are aimed at extracting sets of unique features of an image or a specific object. This is achieved through parallel image processing in different layers of the network using alternating convolution layers (image processing with local operations using filters) and compression (image compression by combining filter values), as well as a fully connected layer that forms the result from the obtained values. As a result, lineaments are identified in the form of short straight segments, which can be interpreted as so-called "mega-cracks" feathering an extended fault structure [*Petrov et al.*, 2010; *Rebetsky et al.*, 2017].

Before the procedure for identifying lineaments using the created neural network, a method of nonlinear directional image filtering was used at the stage of preliminary preparation of the DEM for the most accurate identification of lineaments. In this study, directional filtering was used to improve the boundaries of the gradient transition between pixel values, in order to highlight certain image characteristics based on their frequency associated with the structural features of the territory. Directional image filtering, in accordance with well-known techniques [*Enoh et al.*, 2021; *Paplinski*, 1998; *Suzen and Toprak*, 1998], was performed in four main directions: N–S (0°), NE–SW (45°), E–W (90°), SE–NW (135°), with the construction of corresponding shadow relief schemes in order to emphasize all possible orientations of the structures identified in the image. The study also used the technique for identifying and verifying large fault zones proposed by *Sivkov et al.* [2020]. It is based on the analysis of the spatial position and the creation of density schemes of non-extended lineaments identified automatically by various software tools. For each linear segment of the lineaments identified using a neural network (based on a DEM with a resolution of 1 km/pixel), we calculated and assigned the true azimuth of its strike as an attribute. Based on this attribute, the lineaments were ranked by classes and eight schemes of relative specific densities of linear objects were constructed with a step of 22.50°.

By now, a situation has arisen where most experts in the field of fault tectonics admit the rupture type of rock destruction, but to describe the kinematics of displacement along the formed rupture, they mainly use shear displacement (from the mechanics point of view). In addition, it is assumed that most of the known faults of the Verkhoyan-Kolyma Mesozoic system were initially formed as strike-slip faults and thrusts [*Gusev*, 1979]. To reconstruct the parameters of the regional stress state (RSS), the kinematics of the main faults and the stages of formation of the framework of fault structures based on the interpretation of the identified lineaments, it is necessary to adopt one of the common tectonophysical models of the formation of the paragenesis of the feathering cracks of the main fault (the main structure of the first order on the scale of the study area) in the shear zone. For shear zones (before the formation of the main fault take place), natural patterns of second-order faults have been established and explained from the standpoint of mechanics [*Rebetsky et al.*, 2017; *Seminsky*, 2003]. At the initial stage, in a relatively homogeneous RSS for a certain territory, en echelon systems of tensile cracks (one system) and shear (two conjugate systems) arise. In shear zones, the orientation of cracks in these systems corresponds to the stress state of pure shear [*Gzovsky*, 1975]. If a slight compression or extension across the strike axis of the zone is superimposed on a pure shear, the regional stress state may remain close to a pure shear, but the orientation of the compression and extension axes, as well as the associated orientation of the cracks, change in a regular manner [*Gzovsky*, 1975; *Seminsky*, 2003]. This initial RSS of the shear zones and the cracks that arose as a result of its action can be considered as corresponding to the 1st stage of the development of the main rupture – the stage of its preparation.

There are various explanations for the formation of second-order faults around already active faults from the standpoint of mechanics [*Hancock*, 1985; *Seminsky*, 2003].

P. L. Hancock provides the most complete summary scheme of the series of secondary structures observed in shear zones before the formation of the main fault in them and after its formation [*Hancock*, 1985] (Figure 3). This model was used as the main one in our study.

The software "Lineament Stress Calculator" (author A. D. Svecherevsky, IGEM RAS) was created specifically to solve the tasks of our study to interpret the orientations of the identified lineaments using the P. L. Hancock model. The developed software conducts automatic analysis of linear vector data, identifying and classifying various types of cracks based on their geometric and spatial characteristics. The results of reconstructing the orientation of the axis of the principal compressive or tensile forces in the region for each of the zones of dynamic influence of faults on the assumed period of ore formation allow visualization of segments of structures that are predisposed to shear to varying degrees,
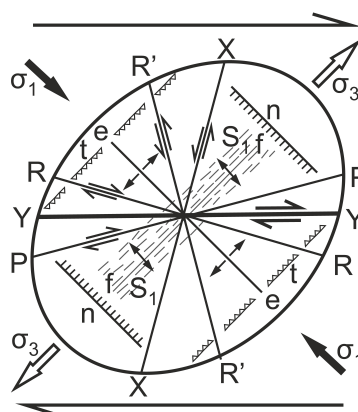
Figure 3. Systems of echelon structural elements formed in a strike-slip fault zone by pure shear [*Hancock*, 1985]: Y – main shear, R and R' – conjugate Riedel shears, X, P – secondary shears, e – tensile cracks, n – normal faults, t – reverse faults, f – folds, S_1 – cleavage, σ_1 – axis of maximum compression, σ_3 – axis of maximum extension.

areas of concentration and dispersion of deformations. Shear stress on the fault plane (τ_n) and effective (σ_n) normal stress can be calculated using the formula [*Jaeger and Cook*, 1979]:

$$\tau_n = \tau \sin 2\varphi \quad \text{when} \quad \tau = \frac{S_1 - S_3}{2},$$

$$\sigma_n = \left(\frac{S_1 + S_3}{2} - P_f\right) + \tau \cos 2\varphi,$$

where S_1 is the stress value along the axis of maximum compression, S_3 is the stress value along the axis of least compression, P_f is the fluid pressure, φ is the angle between the normal to the plane of the fault and the axis of action of the stress S_1 (Figure 4).

The slip tendency (μ) of a certain structural element (segment) of a fault can be calculated as the ratio of shear (tangential) stresses to effective stresses:

$$\mu = \frac{\tau_n}{\sigma_n}.$$

In this case, the most hydraulically active segments of fault structures have $\mu \approx 0.6$ [*Fuchs and Müller*, 2001; *Jaeger and Cook*, 1979].

We used these approaches to reconstruct the framework of faults based on structural and geomorphological features, determine the parameters of RSS, establish the kinematics of the main identified fault zones, identify the most hydraulically active fault segments, and reconstruct the stages of structure formation.

In this case, without reliable information on the values of stresses and fluid pressure, and also taking into account the fact that a significant difference between the values of S_1 and S_3 is required for the formation of a strike-slip fault at $S_1 > S_3$ [*Zobak*, 2010], we adopted the conditional values of $S_1 = 70\,\text{MPa}$ and $S_3 = 20\,\text{MPa}$. In this case, the values of shear stresses at the adopted values of the angle φ reach 25 MPa, which corresponds to the average values of shear stresses for modern settings of intraplate orogenesis, subduction regions and boundaries of lithospheric plates [*Rebetsky et al.*, 2009]. In addition, with such values of S_1 and S_3 for our sample of objects, the values $\mu \leq 0.67$, which simplifies further classification. Considering that the difference between the values of S_1 and S_3 affects the value of μ, we assumed that segments with μ values from 0.45 to 0.67 were hydraulically active. Fluid pressure was ignored in our model as a variable that does not have a significant effect on the final result. According to Yu. L. Rebetsky, fluid pressure is 0.6–0.8 of the lithostatic pressure for modern areas of intraplate orogenesis [*Rebetsky*, 2008].
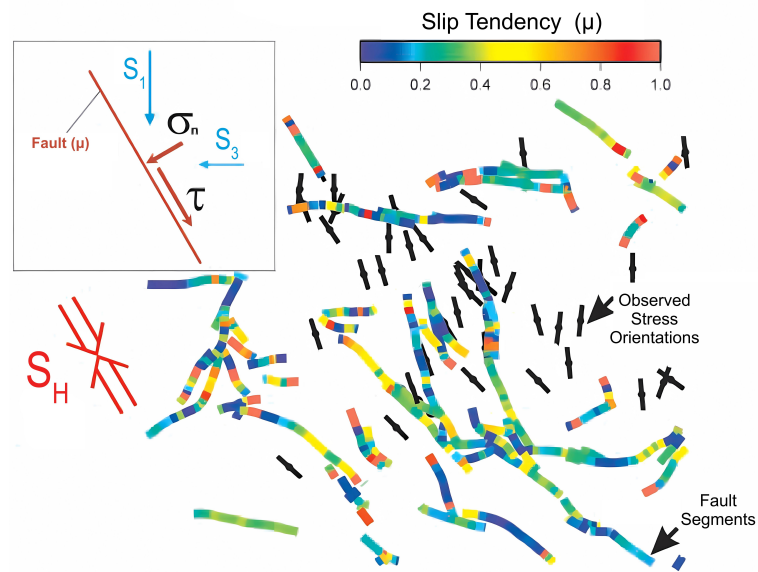
Figure 4. General scheme for determining the slip tendency (μ) based on a combination of orientations of regional anisotropic stresses (black symbols – orientation of the maximum compression axis) with orientations of segments of fault structures with calculation of the ratio of shear (τ) to normal stress (σ_n) for fault segments: S_1 – orientation of the axis of maximum compression, S_2 – axis of minimum compression, S_H – regional orientation of the axis of maximum compression. Segments demonstrating the highest degree of hydraulic activity are indicated in yellow and orange [*Fuchs and Müller*, 2001].

Additional numerical modeling was performed based on the assessment of the acting stresses according to the normalized Mohr diagram [*Rebetskiy et al.*, 2022] taking into account the pore pressure and adjusting the depth of the estimated stress state. As a result of restoring the values of the principal acting stresses, a new ratio was obtained $S_1 = 33\,\text{MPa}$ and $S_3 = 3\,\text{MPa}$ (in comparison with $S_1 = 70\,\text{MPa}$ and $S_3 = 20\,\text{MPa}$ adopted in the article). An additional iteration of modeling showed that:

1. The ratio of the principal acting stresses changed towards a more pronounced stress deviator, which led to an increase in the absolute values of the degree of hydraulic activity of the faults. Nevertheless, the qualitative interpretation based on a relative comparison of the tendency to shift μ (degree of hydraulic activity) has not changed; the same lineaments are distinguished as in the original model.

2. The result of variational modeling with different orientations of the principal axis of compressive stresses showed that its geometry, together with the elements of the occurrence of tectonic faults, determines the degree of hydraulic activity of faults, but not the absolute values of stresses.

Results

As already mentioned, lineaments were automatically identified for the study area based on the DEM (Figure 5)

The approach used, given the high spatial resolution of the DEM, made it possible to identify many short lineaments (6820) in the area.

Considering that the modern morphological appearance of the faults of the Verkhoyansk-Kolyma orogen was acquired in the Mesozoic [*Gusev*, 1979], in order to supplement the framework of faults from the state geological maps (see Figure 2), it was decided to manually identify extended lineaments (while ignoring relatively small ones) based on the DEM (Figure 6). Such lineaments can mark long-lived fault zones. For further operations, the lineaments identified manually are divided into straight segments. A total of 3209 such segments were identified. It can be noted that when selecting both in automatic and

manual mode, the overwhelming majority of lineaments are noted in the western part of the study area, which is associated with the more dissected relief of the Verkhoyan Range, which occupies this area.
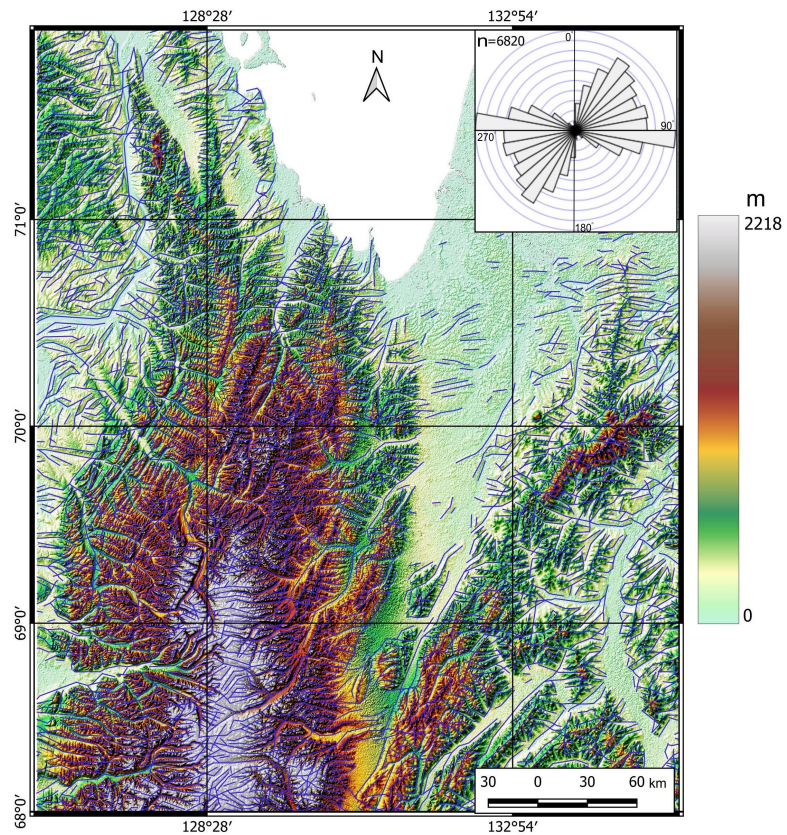

Figure 5. A digital elevation model visualized in GIS with a spatial resolution of 1 km/pixel) with lineaments (blue lines) created by a neural network and rose diagrams of their orientations. The color scale reflects the elevation marks of the relief. *n* – the number of lineaments.

In accordance with the methodology proposed by D. V. Sivkov and co-authors [*Sivkov et al.*, 2020], diagrams of relative specific densities of lineaments were constructed for orientation intervals with identified trends (Figure 7).

All the diagrams show local maxima of the relative specific density of lineaments, which line up in linear "chains" and form some trends. Such trends formed from a set of closely spaced coplanar lineaments. Accordingly, the maxima of the relative specific density lining up, coinciding in azimuth with the lineaments of certain orientations, will mark large linear geological objects, most likely, zones of extended faults.

On the generalized rose diagram of lineament trends (see Figure 7I), the north-eastern striking system is clearly distinguished. In Figures 5 and 6, this system is not so clearly manifested. This can be explained by the fact that the lineaments mostly mark smaller feather structures.

The authors of the article attempted to reconstruct the parameters of the RSS based on the model of *Hancock* [1985] for the main faults of the eastern part of the study area – Emissky, Yansky and Adycha-Tarynsky (see Figure 2). No reconstructions were made for the East Omoloy strike-slip fault because the thick cover of Paleogene-Neogene sediments did not allow for identifying a sufficient number of lineaments in its conditional zone of influence. The reconstruction was based on small lineaments identified automatically. In this case, lineaments identified manually were not used because there were not enough of them within the conditional zones of influence of the faults under study.
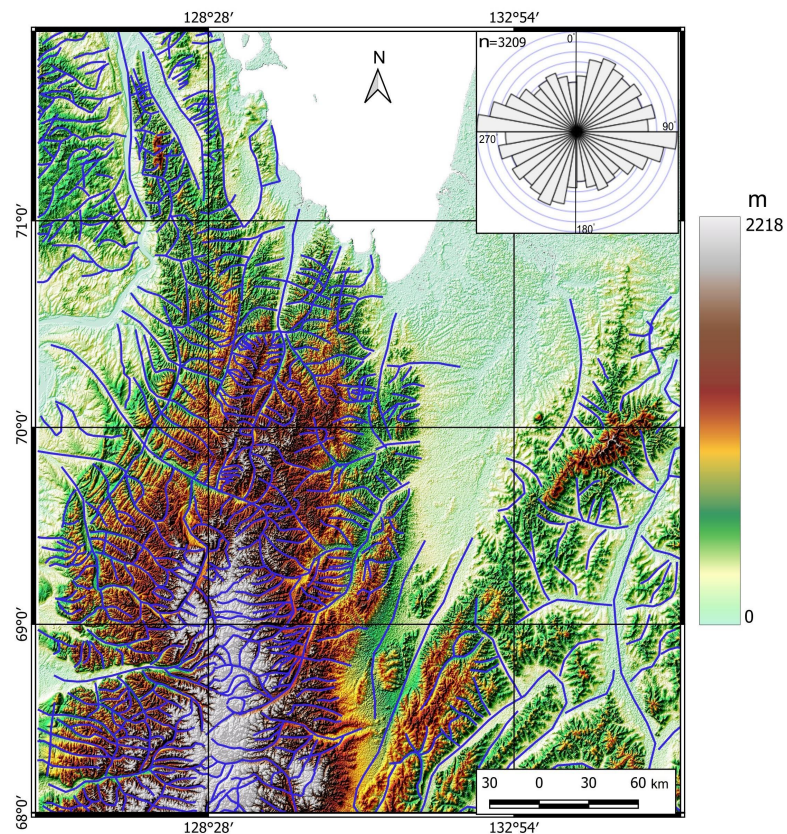
Figure 6. A digital elevation model visualized in GIS with a spatial resolution of 1 km/pixel with manually selected extended lineaments (blue lines) and a rose diagram of their orientations. The color scale reflects the elevation marks of the relief. n – the number of lineaments.

For each of the faults, an individual damage zone of the same name was determined. The damage zones consist of a conventional line ("trend") of the fault under study and the elements of fault tectonics, which can be represented by faults (mega-cracks) of higher orders or lineaments. For the purpose of correct reconstruction, the latter are divided into rectilinear segments. The width (conventional "zone of influence") of the damage zones was determined experimentally, since the traditional concept of a "zone of dynamic influence of a fault" does not quite fit the studied structures of a supraregional scale. For each damage zone, depending on the scale of development of the main structure, the RSS was reconstructed within "zones of influence" of different sizes – from 10 to 100 km. It was established that for both damage zones, the orientations of the principal stresses of the RSS were preserved at a width of the "zone of influence" from 10 km to several tens of kilometers. A change in the orientations of stress axes clearly occurred in the case of mutual overlapping of "zones of influence" of different structures. The boundaries of such a transition were fixed and served in our models as limiters of damage zones in width.

The results of the reconstruction of the parameters of the RSS (Figure 8) show that in all cases in the eastern part of the studied territory the axis of regional compression had an east-northeast orientation ($\approx 65°$), which may indicate uniform conditions for the formation of the faults under consideration and, in general, corresponds to the hypothesis of the connection of their formation in connection with orogenic processes and accretion-collision events of the formation of the South Anyui suture and the New Siberian-Chukotka orogenic belt.

In the western part of the study area, only a few gold ore occurrences are localized (see Figure 2). The main Central Verkhoyansky fault and the Priverkhoyansky marginal suture are located within its boundaries. Both structures extend along the entire western region.
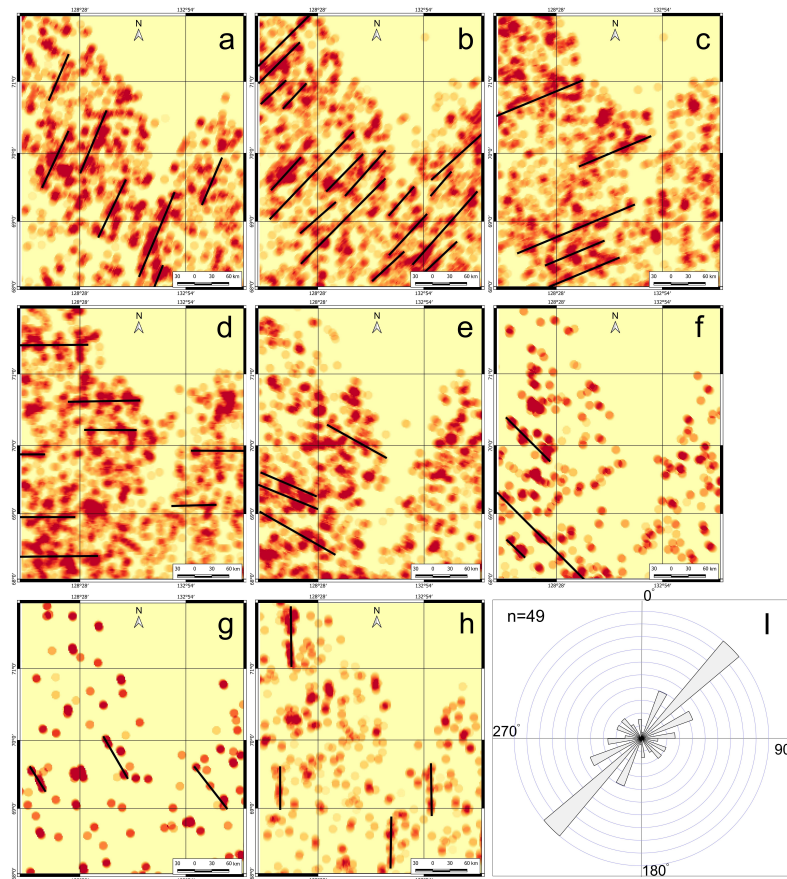
Figure 7. (a)–(h) – schemes of relative specific densities of lineaments by orientation intervals with identified trends (shown as bold black lines) according to the method [*Sivkov et al.*, 2020]: (a) 11–34°; (b) 33.5–56.5°; (c) 56–79°; (g) 78.5–101.5°; (d) 101–124°; (f) 123.5–146.5°; (g) 146–169°; (h) 168.5–11.5°. The color shows the relative specific density of lineaments from 0% (yellow) to 100% (dark red); and (i) generalized rose diagram of the orientation of lineament trends. *n* – the number of objects used to construct the rose diagram.

No reconstruction of the RSS parameters was carried out for the Priverkhoyansky marginal suture, since it is a boundary zone between the Siberian craton and the Verkhoyansk-Kolyma orogenic region and is partially overlapped by a thick cover of Cretaceous sediments. For the Central Verkhoyansky fault, the RSS parameters were reconstructed based on the lineaments identified by automatic and manual methods (Figure 9). As a result, it was revealed that the axis of regional compression during the fault formation was oriented similarly to the eastern part ($\approx 65°$).

Thus, it can be assumed that the regional orientations of the principal RSS axes have been reconstructed for the northwestern part of the Verkhoyansk-Kolyma orogenic region.

Based on the results of reconstructing the orientation of the principal regional compression and extension axes, calculating the slip tendency coefficient (μ), it is possible to visualize segments of established and inferred (lineaments) fault structures, with varying degrees of susceptibility to transtension. The calculations were carried out for faults reflected on the State Geological Map and lineament density trends identified using the methodology [*Hancock*, 1985] as co-scale objects (Figure 10).

Due to the uniform parameters of the reconstructed RSS, calculations of the slip tendency coefficient (μ) were carried out jointly for the entire study area.

As a result, the segments of the structures under consideration are classified from impermeable to highly permeable and presented in a combined diagram (see Figure 10a). For clarity, a diagram of the influence zones of fault segments and segments of permeable
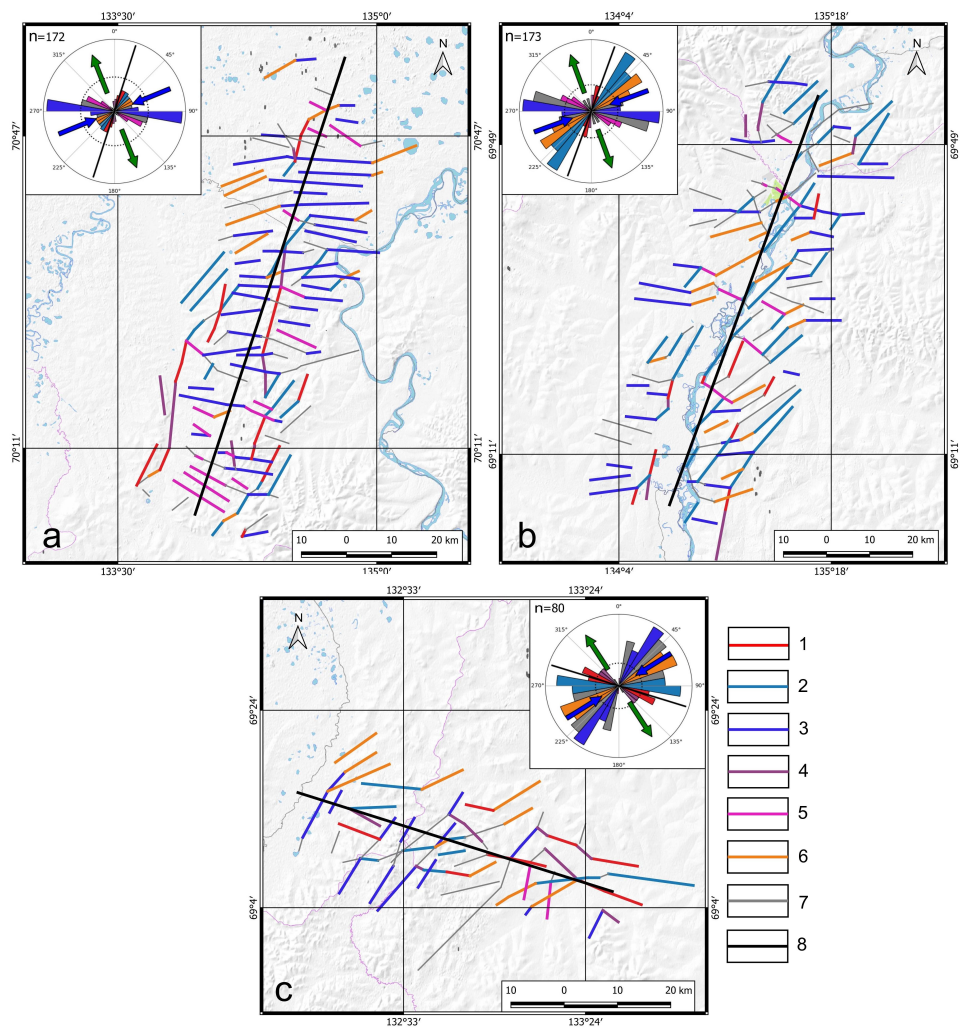
Figure 8. Reconstruction of the parameters of the regional stress state for the Emisskaya (a); Yanskaya (b) and Adycha-Tarynskaya (c) damage zones according to the model of P. L. Hancock based on lineaments identified automatically. 1 – Y-cracks; 2 – R-cracks; 3 – R'-cracks; 4 – P-cracks; 5 – X-cracks; 6 – T-cracks; 7 – not determined; 8 – fault "trend" (shear line). Blue arrows – orientation of the axis of maximum compression; green arrows – orientation of the axis of maximum extension. n – number of objects used to construct the rose diagram.

and high permeability lineament density trends is constructed (see Figure 10b). In this case, the width of the damage zone for all structures is conventionally accepted as 10 km.

From the figures provided, it is clear that, with the exception of several ore occurrences located in lowlands where it is impossible to identify reliable lineaments, all gold ore objects of hydrothermal genesis are located in the conventional zones of influence of permeable and high permeability structures in the Aptian-Albian period, which confirms our calculations.

Conclusions

The following conclusions can be drawn from the results of the study:

1. A comprehensive structural-lineament analysis was carried out for the territory of the northwestern part of the Verkhoyansk-Kolyma orogenic region based on various data, scientific and methodological author's approaches to identifying lineaments using a digital elevation model, including its multidirectional filtering, and the use of geoinformation technologies.

2. Based on the P. L. Hancock model of secondary structures development in the shear zone and the identified faults, the parameters (orientations of the principal stress axes) of the regional stress state, as well as the kinematics of the main faults for the study area for the supposed period of ore formation, were reconstructed. The
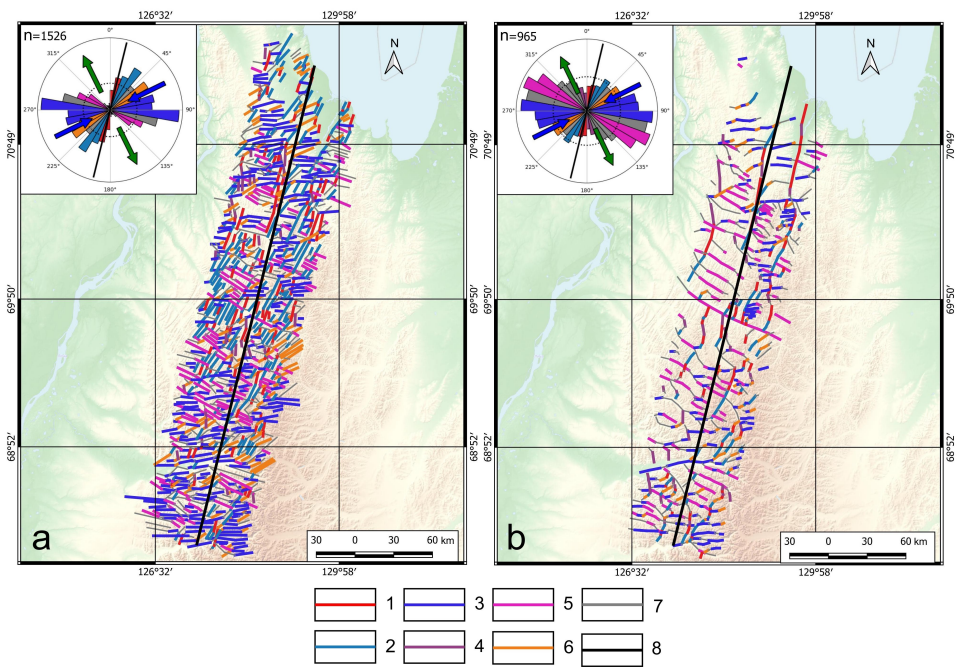
Figure 9. Reconstruction of the parameters of the regional stress state for the Central Verkhoyanskaya damage zone according to the model of P. L. Hancock based on lineaments identified by automatic (a) and manual (b) methods. 1 – *Y*-cracks; 2 – *R*-cracks; 3 – *R'*-cracks; 4 – *P*-cracks; 5 – *X*-cracks; 6 – *T*-cracks; 7 – not determined; 8 – fault "trend" (shear line). Blue arrows – orientation of the axis of maximum compression; green arrows – orientation of the axis of maximum tension. *n* – number of objects used to construct the rose diagram.
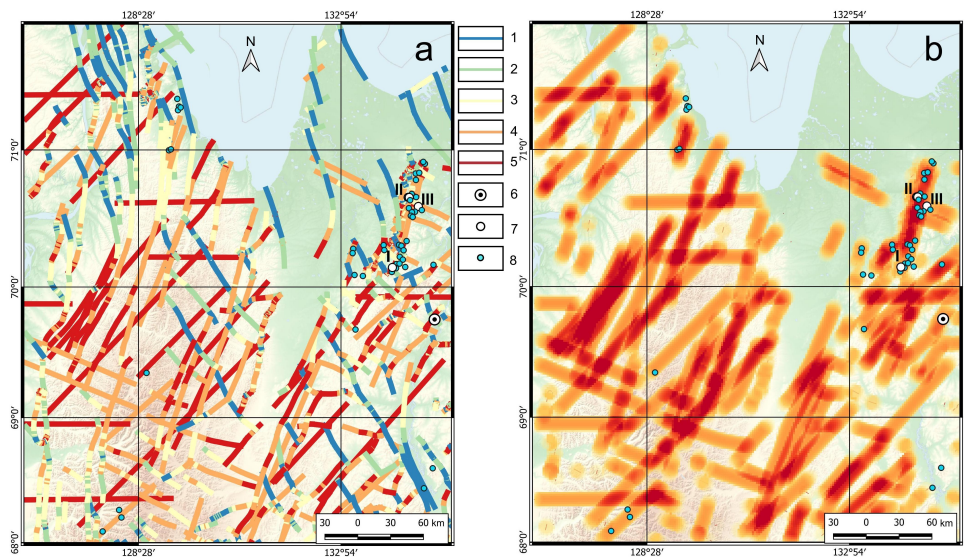

Figure 10. Results of reconstruction of hydraulic activity of segments of tectonic elements: (a) – classified segments of the entire fault network from the State Geological Map and lineament density trends; (b) – diagram of influence zones (orange lines) of fault segments and segments of lineament density trends of permeable and high permeability. Areas of overlapping influence zones of several faults are colored red. 1 – impermeable segments; 2 – low permeability segments; 3 – segments of medium permeability; 4 – permeable segments; 5 – segments of high permeability, 6 – Kyuchus large gold deposit; 7 – small hydrothermal gold deposits (I – Mastakh; II – Emis and Yemelyanovskoye; III – Kyllakh); 8 – hydrothermal gold ore occurrences.

results of the paleoreconstructions correspond to specific tectonic events previously identified by other researchers [*Prokopiev et al.*, 2018].

3. Calculation of the slip tendency (transtension) coefficient taking into account the established orientation of the principal axes of the regional stress state allowed us to identify the most hydraulically active segments of fault structures that correspond to north-northeast, northeast, sublatitudinal and west-northwest orientations.

4. From the point of view of predicting the location of gold ore deposits, further detailed work should be focused on studying the zones of influence of hydraulically active faults. These supraregional and regional structures could act as fluid pathways in the process of hydrothermal ore formation.

References

Antonov A. E. and Gamyanin G. N. Deposits of strategic metals of the Arctic region // Gold and technology. — 2021. — 1 (51). — URL: https://zolteh.ru/regions/sverkhkrupnye_mestorozhdeniya_zolota_rossii_i_uzbekistana_perspektivy_novykh_otkryti/ ; (in Russian).

Borisova T. P., Gertseva M. V. and Egorov A. Yu. State Geological Map of the Russian Federation, scale 1:1,000,000. Verkhoyansk-Kolyma Series. R-52 (Tiksi). — St. Petersburg, 2016. — (In Russian).

Borisova T. P., Gertseva M. V. and Egorov A. Yu. State Geological Map of the Russian Federation, scale 1:1,000,000. Verkhoyansk-Kolyma Series. R-53 (Nizhneyansk). — St. Petersburg, 2020. — (In Russian).

Cherezov A. M., Shirokih I. N. and Vaskov A. S. Structure and zoning of hydrothermal deposits in fault zones. — Novosibirsk : Nauka. Siberian Publishing Company, 1992. — P. 104. — (In Russian).

Enoh M. A., Okeke F. I. and Okeke U. C. Automatic lineaments mapping and extraction in relationship to natural hydrocarbon seepage in Ugwueme, South-Eastern Nigeria // Geod. Cartogr. — 2021. — Vol. 47. — P. 34–44. — https://doi.org/10.3846/GAC.2021.12099.

Fuchs K. and Müller B. World Stress Map of the Earth: a key to tectonic processes and technological applications // Naturwissenschaften. — 2001. — Vol. 88, no. 9. — P. 357–371. — https://doi.org/10.1007/s001140100253.

Grishkov G. A., Nafigin I. O., Ustinov S. A., et al. Developing a Technique for Automatic Lineament Identification Based on the Neural Network Approach // Izv. Atmos. Ocean. Phys. — 2023. — Vol. 59. — P. 1271–1280. — https://doi.org/10.1134/S0001433823120101.

Gusev G. S. Folded structures and faults of the Verkhoyansk-Kolyma system of Mesozoids. — Nauka, 1979. — P. 208. — (In Russian).

Gzovsky M. V. Fundamentals of Tectonophysics. — Moscow : Nauka, 1975. — P. 536. — (In Russian).

Hancock P. L. Brittle microtectonics: principles and practice // Journal of Structural Geology. — 1985. — Vol. 7, no. 3/4. — P. 437–457. — https://doi.org/10.1016/0191-8141(85)90048-3.

Jaeger J. C. and Cook N. G. W. Fundamentals of Rock Mechanics. Third edition. — Chapman, Hall, 1979. — 593 p.

Konstantinovsky A. A. Structure and geodynamics of the Verkhoyansk Fold-Thrust Belt // Geotectonics. — 2007. — Vol. 41, no. 5. — P. 337–354. — https://doi.org/10.1134/s0016852107050019.

Kungurtsev L. V. and Goshko E. Y. Deep Structure and Formation Model of Continental Crust of the Verkhoyansk Fold-and-Thrust Belt in the Late Mesozoic // Geodynamics & Tectonophysics. — 2023. — Vol. 14, no. 3. — P. 0706. — https://doi.org/10.5800/GT-2023-14-3-0706. — (In Russian).

Minaev V. A., Ustinov S. A., Petrov V. A., et al. Regional Remote Sensing Analysis of Fault Tectonics of the Kola Peninsula and Its Role in Ore Formation // Russian Journal of Earth Sciences. — 2024. — Vol. 24. — ES3010. — https://doi.org/10.2205/2024es000918. — (In Russian).

Paplinski A. Directional filtering in edge detection // IEEE Trans. Image Processing. — 1998. — Vol. 7. — P. 611–615.

Petrov V. A., Sim L. A., Nasimov R. M., et al. Fault tectonics, neotectonic stresses, and hidden uranium mineralization in the area adjacent to the Strel'tsovka Caldera // Geology of Ore Deposits. — 2010. — Vol. 52, no. 4. — P. 279–288. — https://doi.org/10.1134/S1075701510040033.

Prokopiev A. V., Borisenko A. S., Gamyanin G. N., et al. Age constraints and tectonic settings of metallogenic and magmatic events in the Verkhoyansk-Kolyma folded area // Russian Geology and Geophysics. — 2018. — Vol. 59, no. 10. — P. 1237–1253. — https://doi.org/10.1016/j.rgg.2018.09.004.

Rebetskiy Yu. L., Sim L. A. and Marinin A. V. Algorithm for calculating neotectonic stresses in platform areas by the structural-geomorphological method // Geodynamics & Tectonophysics. — 2022. — Vol. 13, no. 1. — https://doi.org/10.5800/gt-2022-13-1-0577. — (In Russian).

Rebetsky Yu. L. Mechanism of tectonic stress generation in the zones of high vertical movements // Fizicheskaya Mezomekhanika. — 2008. — Vol. 11, no. 1. — P. 66–73. — EDN: IJRQTF ; (in Russian).

Rebetsky Yu. L., Kuchai O. A. and Sycheva N. A. Method of cataclastic analysis of faults and results of calculations of the modern stress state in the crust near plate boundaries and for intraplate mountain-folded orogens // Tectonophysics and current issues of Earth sciences. On the 40th anniversary of the establishment of the tectonophysics laboratory at the IPE RAS by M.V. Gzovsky: Proceedings of the All-Russian Conference (October 13-17, 2008). Volume 1. — Moscow : IPE RAS, 2009. — P. 340–366. — EDN: XXCINF ; (in Russian).

Rebetsky Yu. L., Sim L. A. and Marinin A. V. From slickensides to tectonic stresses. Methods and algorithms. — Moscow : GEOS, 2017. — 235 p. — EDN: YPNZQR ; (in Russian).

Seminsky K. Zh. Internal structure of continental fault zones: tectonophysical aspect. — Novosibirsk : Institute of the Earth's Crust of the Siberian Branch of the Russian Academy of Sciences, 2003. — 243 p. — EDN: WPMWBH ; (in Russian).

Sivkov D. V., Chitalin A. F. and Dergachev A. L. Using Lineament Analysis to Identify Patterns in the Localization of Au Mineralization in the Taryn Gold Field in the Republic of Sakha (Yakutia) // Izvestiya, Atmospheric and Oceanic Physics. — 2020. — Vol. 56, no. 12. — P. 1546–1559. — https://doi.org/10.1134/s0001433820120543. — (In Russian).

Suzen M. L. and Toprak V. Filtering of satellite images in geological lineament analyses: An application to a fault zone in Central Turkey // International Journal of Remote Sensing. — 1998. — Vol. 19, no. 6. — P. 1101–1114. — https://doi.org/10.1080/014311698215621.

Ustinov S. A., Chepchugov A. M., Tomarovskaya M. A., et al. Structural-Tectonophysical Approach to Interpretation of Lineament Analysis Results for Prediction of Ore-Forming Mineral Systems on the Example of the Tuyukansky Ore Cluster Area // Issledovanie Zemli iz kosmosa. — 2024. — No. 5. — P. 35–57. — https://doi.org/10.31857/S0205961424050037. — (In Russian).

Ustinov S. A. and Petrov V. A. Use of Detailed Digital Relief Models for the Structural and Lineament Analysis (on Example of the Urtuysky Granite Massif, SE Transbaikalia) // Geoinformatica. — 2016. — No. 2. — P. 51–60. — (In Russian).

Volkov A. V. Golden Heart of Siberia // Gold and Technology. — 2016. — 2 (32). — P. 42–48. — (In Russian).

Zobak M. D. Reservoir Geomechanics. 1st edition. — Cambridge University Press, 2010. — 461 p.